HHS Public Access

Author manuscript

Oncogene. Author manuscript; available in PMC 2021 June 15.

Published in final edited form as:

Oncogene. 2021 February ; 40(6): 1064–1076. doi:10.1038/s41388-020-01582-8.

Pten-NOLC1 Fusion Promotes Cancers Involving MET and EGFR Signalings

Jian-Hua Luo[±,*], **Silvia Liu**[±], **Junyan Tao**[±], **Bao-Guo Ren**[±], **Katherine Luo**[1], **Zhang-Hui Chen**[±], **Michael Nalesnik**[±], **Kathleen Cieply**[±], **Tianzhou Ma**[2], **Shi-Yuan Cheng**[3], **Qi Chen**[4], **George K. Michalopoulos**[±], **Joel B. Nelson**[5], **Rohit Bhargava**[±], **Jun Zhang**[6], **Deqin Ma**[7], **David Jarrard**[8], **Arjun Pennathur**[9], **James D. Luketich**[9], **Donald B. DeFranco**[10], **Satdarshan Paul Monga**[±], **George Tseng**[1], **Yan-Ping Yu**[±,*]

[1]Department of Biology, Columbia University, 1212 Amsterdam Avenue; New York, NY 10027

[2]Department of Biostatistics, University of Pittsburgh School of Medicine, Pittsburgh, PA 15261

[3]Department of Neurology, Northwestern University School of Medicine, Chicago, IL 60611

[4]Department of Pharmacology, Toxicology & Therapeutics, University of Kansas, Kansas City, KS 66160

[5]Department of Urology, University of Pittsburgh School of Medicine, Pittsburgh, PA 15261

[6]Department of Medicine, University of Iowa, Iowa City, Iowa 52242

[7]Department Pathology, University of Iowa, Iowa City, Iowa 52242

[8]Department of Urology, University of Wisconsin Madison, Madison, WI 53792

[9]Department of Thoracic Surgery, University of Pittsburgh School of Medicine, Pittsburgh, PA 15261

[10]Department of Pharmacology, University of Pittsburgh School of Medicine, Pittsburgh, PA 15261

[±]Department of Pathology, University of Pittsburgh School of Medicine, Pittsburgh, PA 15261

Abstract

Inactivation of *Pten* gene through deletions and mutations leading to excessive pro-growth signaling pathway activations frequently occurs in cancers. Here, we report a *Pten* derived pro-cancer growth gene fusion *Pten-NOLC1* originated from a chr10 genome rearrangement and identified through a transcriptome sequencing analysis of human cancers. *Pten-NOLC1* fusion is present in primary human cancer samples and cancer cell lines from different organs. The product of *Pten-NOLC1* is a nuclear protein that interacts and activates promoters of *EGFR, c-MET, and their signaling molecules.* Pten-NOLC1 promotes cancer proliferation, growth, invasion, and metastasis, and reduces the survival of animals xenografted with Pten-NOLC1-expressing cancer

*- To whom correspondence should be addressed: Jian-Hua Luo, Department of Pathology, University of Pittsburgh School of Medicine, Scaife S-728, 3550 Terrace Street, Pittsburgh, PA 15261; luoj@msx.upmc.edu. Yan-Ping Yu, Department of Pathology, University of Pittsburgh School of Medicine, Scaife S-756, 3550 Terrace Street, Pittsburgh, PA 15261; ypyu@pitt.edu.

All authors declare no conflict of interest in the study

cells. Genomic disruption of *Pten-NOLC1* induces cancer cell death, while genomic integration of this fusion gene into the liver coupled with somatic *Pten* deletion produces spontaneous liver cancers in mice. Our studies indicate that *Pten-NOLC1* gene fusion is a driver for human cancers.

Introduction:

Chromosome rearrangement is one of the critical features of human cancers[1, 2]. This genome aberration may result in gene fusion by joining the genes far apart in the chromosome position or different orientations to form a chimeric transcription unit. Most breakpoints of the gene fusions are located in the introns of the involving genes. The consequences of gene fusion include gene truncation, chimera protein generation, or complete elimination of the tail gene product due to frameshift[3]. Some fusion genes are organ-specific such as *BCR-Abl*[4], *TMPRSS2-ERG*[5], and *PAX8-PPARG*[6], while others are widely present across multiple types of human cancers such as *MAN2A1-FER*[7]. Many fusion genes are drivers in human cancer development.

Pten[8, 9] is a tumor suppressor in many human cancers. It dephosphorylates phosphatidylinositol (3,4,5)-trisphosphate (PIP_3)[10, 11] to maintain homeostatic PI3K/AKT signaling and is a crucial regulator of cell survival and growth[12, 13]. Polyubiquitination of Pten leads to the inactivation of Pten in the cytosol, while monoubiquitination leads to the nuclear translocation of Pten[14, 15]. In a variety of human malignancies, *Pten* deletion and mutation are among the most crucial driver events for cancer development[16]. *NOLC1* is a highly phosphorylated nucleolus coiled protein and a binding protein for RNA polymerase I[17]. *NOLC1* is essential for small nucleolar riboprotein synthesis[18, 19] and a critical transcription factor for an array of gene transcriptions[20–23]. Here, we report a novel gene fusion between *Pten* and *NOLC1*. The gene fusion creates an oncogenic chimera protein with a Pten domain in the N-terminus and a NOLC1 domain in the C-terminus. Our finding indicates that *Pten-NOLC1* promotes tumorigenesis both *in vitro* and *in vivo*.

Results:

The Pten-NOLC1 fusion protein is a product of chromosome 10 rearrangement

Pten-NOLC1 fusion transcripts were identified through transcriptome sequencing analysis of 107 prostate samples (20 organ donor prostate samples, three benign prostate samples from cancer-adjacent regions, and 84 prostate cancer (PCa) samples) with ultradeep sequencing coverage (up to 2000x). Among the ninety-six cancer-specific fusion transcripts recognized by the FusionCatcher algorithm (Supplemental Table 1), the *Pten-NOLC1* fusion gene is one of the six fusion genes validated in our subsequent studies (figure 1 and supplemental figures 1–2). *Pten-NOLC1* results from the fusion of two genes, *Pten* (10q23.3) and *NOLC1* (10q24.32), 14.2 Mbp apart in chromosome 10 through chromosomal rearrangement. *Pten* is a tumor suppressor that negatively regulates PI3K-AKT activities in the cytoplasm[8] and complexes with P300 to activate p53 in the nucleus[17, 24, 25]. *NOLC1* is a nucleolar and coiled-body phosphoprotein promoting nucleolar organogenesis[24].

The predicted translation product of *Pten-NOLC1* fusion transcript is a Pten chimeric protein: A truncated NOLC1 sequence (aa 41-699) containing its most functional domains and nuclear localization signals replaces the 62 amino acids of Pten C2 domain at the C-terminus. To validate the results from transcriptome sequencing, we performed Taqman qRT-PCR and Sanger sequencing analysis of the PCR product from samples positive for *Pten-NOLC1* and found the juncture sequences of *Pten-NOLC1* fusion transcripts in these samples (figure 1A).

To determine whether *Pten-NOLC1* is a transcriptional product of a rearranged genome, we performed the FISH analysis to examine whether the recombination of *Pten* and *NOLC1* genes was present in the chromosome 10 of PCa samples positive for *Pten-NOLC1* fusion transcripts. As shown in figure 1B, the probes corresponding to the 5' end of *Pten* gene (Spectrum Orange) and 3' end of *NOLC1* (Spectrum Green) hybridized to the PCa cells, producing overlapping hybridization signals (yellowish), indicating that these two genes, *Pten* and *NOLC1*, were fused. Independent *NOLC1* signals (green) were visible in the same cancer cells, while wild-type *Pten* signals (red) were absent. In the normal organ donor prostate tissue, two distinct pairs of separate signals for *Pten* and *NOLC1* were both visible. The coexistence of *Pten-NOLC1* genomic recombination and hemizygous *Pten* deletion in the cancer genome suggests a complete functional loss of both alleles of *Pten* in this cancer sample.

To identify the genomic breakpoint of *Pten-NOLC1*, we performed a series of long-extension PCRs on genomic DNA from the PCa sample using primers corresponding to the genomic sequences flanking the fusion juncture (see the Methods section). As shown in figure 1C, sequence analysis of the PCR product yielded the sequence of the chromosomal breakpoint of *Pten-NOLC1*, located at a region between intron 8 of *Pten* and intron 1 of *NOLC1*. The breakpoint contains an 8 bp (TAGCTGGG) overlapping sequence shared by *Pten* and *NOLC1* introns. The human cancer cell lines, including LNCaP, DU145, H1299, VCaP, HEP3B, MCF7, and PC3, showed the same breakpoint, although these cells were the malignancies from different organs and had dfferent biological features. The results suggest a common mechanism underlying *Pten-NOLC1* gene recombination in human cancers.

Pten-NOLC1 fusion is prevalent in human malignancies

To investigate whether human cancers frequently express *Pten-NOLC1* fusion gene, we performed TaqMan RT-PCR analyses of *Pten-NOLC1* fusion on 26 human cancer cell lines using fusion juncture-spanning primers and probes. Unexpectedly, we found *Pten-NOLC1* fusion signals in all analyzed cancer cell lines (figure 2A and supplemental figure 3A), including PCa (PC3, DU145, LNCaP, and VCaP), lung cancer (H358, H1299, H522 and H23), breast cancer (MDA-MB231, VACC3133, MDA-MB330, MCF7), liver cancer (HUH7, HEP3B, SNU449, SNU475, SNU375, SNU182, and HEPG2), glioblastoma (A-172, LN229, T98G, U138, and U118), and colon cancer (HCT8 and HCT15) cell lines but not in 20 normal prostate samples from organ donors and 10 matched post-surgery blood samples of patients with PCa (supplemental figure 3B). We further analyzed the existence of *Pten-NOLC1* in primary human cancers by Taqman qRT-PCR screening on 1030 samples of different types of human tumor tissues obtained from six institutes (UPMC, Stanford

University, University of Wisconsin, University of Iowa, Northwestern University and University of Kansas). The results of TaqMan RT-PCR and Sanger sequencing analyses in figure 2B indicate that *Pten-NOLC1* expression was present in 70-85% of these cancer samples: 70.1% (337 of 481) of PCa, 83% (50 of 60) of breast cancer, 75% (45 of 60) of colon cancer, 83% (127 of 153) of glioblastoma multiforme (GBM), 82.9% (58 of 70) of liver cancer, 75.2% (109 of 145) of non-small cell lung cancer (NSCLC), 70.5% (43 of 61) of ovarian cancer and 85% (29 of 34) of esophageal adenocarcinoma samples (figure 2B, Supplemental figure 4 and Supplemental tables 2–9). The FISH analyses were performed on 22 human cancer cell lines and 12 cases of primary human cancers, including NSCLC, HCC, breast cancer and ovarian cancer, all known to be positive for *Pten-NOLC1* fusion transcript. The results confirmed the chromosome rearrangement in Pten/NOLC1 regions of chromosome 10 (Supplemental figure 5).

Northern hybridization revealed a 5.6 Kb transcript from H1299 cells hybridized to both probes corresponding to *Pten* and *NOLC1* (supplemental figure 6A). To investigate the full-length coding sequence of the *Pten-NOLC1* transcript, we performed a series of nested PCRs with primers spanning the junction at different locations on the fusion. We identified *Pten-NOLC1* cDNA fragments of various lengths in Du145 cells via reverse transcription using a primer specific for the 3' end of *NOLC1* (Supplemental figure 6B). The sequence alignments of these PCR fragments predicted the presence of the 3.1 kb full-length coding sequence of *Pten-NOLC1* in the cancer cells. We subsequently examined whether the Pten-NOLC1 chimeric protein was present in the cancer cell lines and primary cancer samples by Western blot (WB) analysis using antibodies specific for Pten (aa 3-29) or NOLC1 (aa 620-699). The Pten-NOLC1 chimeric protein contains epitopes recognizable by both the anti-NOLC1 and anti-Pten antibodies, while wild-type Pten and NOLC1 proteins contain only one of the two epitopes. As shown in figure 2C–D and supplemental figure 7, a 110 kDa protein band, in addition to the Pten band, was present in the immunoblots of 25 cell lines, including H522, HUH7, PC3, DU145, and A-172 and PCa tissues detected with the Pten-specific antibody. However, this 110 kDa band was not present in the immunoblots of samples with a Pten-specific antibody (aa 388-400) against the C-terminal epitope (Supplemental figure 8A). In addition, this band was absent in organ donor prostate samples and non-cancer cell lines (figure 2D and supplemental figure 7). With the antibody specific for NOLC1 epitope, a similar 110 kDa protein band was found in these cancer cell lines and PCa tissues, in addition to the 130 kDa NOLC1 protein band, while no such band was detected in the normal prostate organ donor samples. To verify Pten-NOLC1 fusion found by Western blot analysis, we performed immunoprecipitation on the protein extract from Du145 cells using the Pten-specific antibody and immunoblotted the immunoprecipitate with an antibody specific for NOLC1. As shown in figure 2E, the anti-NOLC1 antibody recognized a protein band of the same size as the 110 kDa band found in the Western blot. Conversely, Pten antibody recognized the similar 110 kDa band from the immunoprecipitate of NOLC1 antibody, which was confirmed to contain NOLC1 and Pten peptides by Mass Spectrometry analysis. Furthermore, the 110 kDa protein band was absent in the *Pten-NOLC1* gene knockout cells (figure 2F) and in the *Pten-NOLC1* knockout clone rescued with $\Delta Pten^{aa1\text{-}342}$ or $\Delta NOLC1^{aa41\text{-}699}$ (Supplemental figure 8B) but reappeared in the clone rescued with *Pten-NOLC1*-3xflag. Taken together, we concluded that the 110 kDa protein

recognized by both the anti-Pten and anti-NOLC1 antibodies was a *Pten-NOLC1* gene product.

Pten-NOLC1 is localized in the nucleus

Pten functions in both the cytosol and nucleus, while NOLC1 is an exclusively nucleolar protein. To examine whether Pten-NOLC1 is localized in any of these locations, we performed immunostaining on NIH3T cells expressing p*CDNA4-Pten-NOLC1-FLAG* with an antibody specific for FLAG (Supplemental figure 8C). As shown in figure 3A, the Pten-NOLC1-FLAG signal was localized exclusively in the nuclei, similar to the NOLC1 signal, in contrast to the diffuse Pten distribution signal. To directly visualize the distribution of Pten-NOLC1 and the impact of Pten or NOLC1 domains on the subcellular localization of Pten-NOLC1, we transfected the vectors into PC3 cells to express Pten-NOLC1-EGFP, Pten-NOLC1-mCherry or $\Delta Pten^{aa1\text{-}342}$-EGFP, or $\Delta NOLC1^{aa41\text{-}699}$-mCherry fluorescent chimeric proteins (Supplemental figure 8C). As shown in figure 3B, the Pten-NOLC1-EGFP signal was localized exclusively in the nuclei and nucleolus of PC3 cells (upper right in figure 3B), similar to the Pten-NOLC1-mCherry signal (the nuclear signals are referenced to the cytoplasmic staining of F-actin by Alexa Fluor 488®-phalloidin, lower right). The $\Delta Pten^{aa1\text{-}342}$-EGFP signal was again diffused throughout the cytoplasm (upper left), in contrast to the DAPI signal from nuclear staining (lower left). The $\Delta NOLC1^{aa41\text{-}699}$-mCherry signal was localized in the nucleus, as referenced to the cytoplasmic F-actin signal (lower middle). Collectively, these results indicate that Pten-NOLC1 and $\Delta NOLC1^{aa41\text{-}699}$ exhibited very similar exclusively nuclear localization, while $\Delta Pten^{aa1\text{-}342}$ exhibited mostly cytosolic but occasional nuclear localization in mitotic cells (figure 3B, 2nd panel from the left).

To verify the presence of nuclear Pten-NOLC1, we fractionated lysates of DU145 cells to examine whether the protein represented by the 110 kDa protein band identified in the cancer cells was localized in the nuclear fraction. As shown in figure 3C, the cytoplasmic fraction produced a 50 kDa band of Pten detected with a Pten-specific antibody (aa 3-29), and the nuclear fraction/nucleolus fraction, produced a 110 kDa band detected with the same Pten-specific antibody. Immunoblotting with the NOLC1-specific antibody revealed a 110 kDa Pten-NOLC1 band in addition to a 130 kDa NOLC1 protein band found exclusively in the nuclear fraction. Truncation of Pten ($\Delta Pten^{aa1\text{-}342}$- FLAG) or NOLC1 ($\Delta NOLC1^{aa41\text{-}699}$-FLAG) did not impact their subcellular localization (Supplemental figure 8D). Collectively, these results demonstrate that the Pten-NOLC1 fusion protein is a 110 kDa nuclear protein immunoreactive with antibodies specific for either Pten (aa 3-29) or NOLC1 (aa 620-699). In addition, nucleolar fractionation and immunostaining showed that significant amount of Pten-NOLC1 is present in nucleolus of DU145 cells (Supplemental figure 9A and B).

Pten-NOLC1 promotes cancer growth and proliferation and increases tumor survival

Pten-NOLC1 has weak to moderate expression in many cancers of different origins and lacks phospholipid phosphatase activity (see Figure 3D, supplemental figure 10A–C and supplemental results and discussion). To investigate whether Pten-NOLC1 expression was imperative to cancer survival and growth, we knocked out *Pten-NOLC1* in DU145, MCF7, and H1299 cells using the CRISPR/$Cas9^{D10A}$ genome editing method [7, 26, 27] by an

inserting a promoterless *zeocin-mCherry* cDNA sequence into the breakpoint region of *Pten-NOLC1* (figure 4A). TaqMan RT-PCR analysis of these knockout clones revealed that the expression of Pten-NOLC1 was disrupted (figure 4B and supplemental figure 11), and the 110 kDa Pten-NOLC1 band was not visible in the Western blot analysis with antibodies specific for either Pten or NOLC1 (figure 4C). The *Pten-NOLC1* knockout cell grew significantly slower than their corresponding parental controls, producing 8- to 13-fold fewer colonies for DU145 cells ($p<0.05$), 2.4-fold fewer colonies for MCF7 cells ($p<0.05$), and 4.5-fold fewer colonies for H1299 cells ($p<0.05$) (figure 4D). Regaining the Pten-NOLC1 expression by transfection of *pCMV-Pten-NOLC1-FLAG*, Pten-NOLC1 knockout clones of DU145 and MCF7 were partially reinvigorated: forming colonies significantly more than DKO1 and MKO1 cells (figure 4D). Neither DKO1+ $\Delta Pten^{aa1\text{-}342}$ (the clone rescued with truncated Pten) nor DKO1+ $\Delta NOLC1^{aa41\text{-}699}$ (the clone rescued with truncated NOLC1) cells showed significantly increased colony formation (Supplemental figure 12A) compared with that of the corresponding controls. Forced expression of Pten-NOLC1 in NIH3T3 and PC3 cells increased the colony numbers by 2.83-fold for NIH3T3 cells and 2.8-fold for PC3 cells, respectively (Supplemental figure 12B).

To test whether the slow growth of *Pten-NOLC1* knockout clones was the result of the slower proliferation of these cells, we performed BrdU cell cycle analyses. As shown in figure 4E, the percentage of the cell populations entering S phase decreased from 23.3% (DU145) to 13% ($p<0.05$) for DKO1 clones with *Pten-NOLC1* disruption and to 8% ($p<0.05$) for DKO2 clones. A similar delay in S phase entry, indicated by a reduction in the percentage of S-phase cells from 23% to 15% ($p<0.05$), was observed in a knockout clone of MCF7 (MKO1), and a decrease from 17% to 7% was observed in an H1299 knockout clone (HKO5). Forced expression of Pten-NOLC1 in NIH3T3 and PC3 cells (Supplemental figure 13A) resulted in an early S phase entry, as evidenced by the increase in the percentage of S-phase cells from 7% to 26% for NIH3T3 cells ($p<0.05$) and from 9% to 32% for PC3 cells ($p<0.05$).

To examine whether Pten-NOLC1 was crucial for cell viability, we performed UV-induced cell death analyses in DU145 and MCF7 and the corresponding *Pten-NOLC1* knockout cells. As shown in figure 4F, 76% of DKO1 cells died when treated with UV irradiation (200MJ) ($p<0.05$) versus 51% of parental cells, suggesting that the presence of Pten-NOLC1 increases the resistance of cells to damage caused by UV radiation. Without Pten-NOLC1, cell vulnerability to UV radiation increased, resulting in a decrease in the ED50 from 191 MJ to 103 MJ for DU145 cells and from 224 MJ to 127 MJ for MCF7 cells (Supplemental figure 13B).

We next examined whether Pten-NOLC1 was essential to the aggressiveness of cancer cells by analyzing the migration and invasion of these cells in Matrigel invasion chambers. As shown in figure 4G, without Pten-NOLC1, the invasion index in the tumor cells reduced by 3.8- and 4-fold for DKO1 and DKO2 cells and by 4-fold HKO5 cells, respectively. Similarly, xenografts of DU145 or H1299 cells and their knockout counterparts in SCID mice showed divergent growth patterns. DU145 tumors overgrew, reaching a tumor volume of 6.3 cm^3 in the sixth week (figure 4H), while DU145 tumors with *Pten-NOLC1* knockout were an average of three times smaller. Most of the mice with DU145 tumors had abdominal,

vertebral, and renal metastatic lesions, while metastasis occurred in only one of the knockout groups (figure 4I). Eighty percent of animals with DU145 tumors died in 7 weeks, while all animals with DKO1 and DKO2 tumors survived through the same period. H1299 xenografts in SCID mice had a 4-week delay before developing into visible tumors. However, the tumor xenografts then began to grow rapidly. Similar to DU145 tumors, wild-type H1299 tumors grew much faster than *Pten-NOLC1* knockout HKO5 tumors. No mice with either H1299 or HKO5 tumors died over the seven weeks, but the average size of the H1299 tumors was four times larger (>4-fold, $p<0.001$, Supplemental figure 14A) than that of the HKO5 tumors. H1299 tumors metastasized to the abdominal cavity, muscles, and vertebrae, while none of the seven HKO5 tumors metastasized ($p<0.001$, Supplemental figure 14A). When Pten-NOLC1 expression was restored in DKO1 cells by pCMV-Pten-NOLC1-FLAG transfection, the xenografted DKO1+Pten-NOLC1-FLAG tumors recovered the growth and aggressiveness of the DU145 tumors (figure 4H). Cancer metastasis occurred in all (7/7) animals with DKO1+Pten-NOLC1 xenograft tumors (figure 4I). DKO1 cells rescued with the truncated Pten (DKO1+ $\Delta Pten^{aa1\text{-}342}$) or truncated NOLC1 (DKO1+ $\Delta NOLC1^{aa41\text{-}699}$) generated tumors with sizes similar to those of the DKO1 tumors (figure 4H). However, animals xenografted with DKO1+ $\Delta Pten^{aa1\text{-}342}$ cells had some metastases. Mice xenografted with DKO1+Pten-NOLC1 cells, and the corresponding parental DU145 cells had similar mortality rates, significantly higher than those of mice xenografted with DKO1, DKO1+$\Delta Pten^{aa1\text{-}342}$, or DKO1+$\Delta NOLC1^{aa41\text{-}699}$ cells (figure 4J and Supplemental figure 14B). MCF7 cells failed to migrate through the Matrigel and to develop tumors in SCID mice. In summary, all xenograft tumors consistently lost their robust growth when *Pten-NOLC1* was knocked out in the cancer cells, and only regain their aggressiveness after the re-introduction of Pten-NOLC1 expression, suggesting that Pten-NOLC1 is a crucial factor in cancer aggressiveness.

Pten-NOLC1 regulates the gene expressions of *c-MET*, *GAB1*, and *EGFR*

NOLC1 is a cofactor of RNA polymerase I[17] and also a cotranscription factor[20, 28]. To elucidate the mechanism of Pten-NOLC1 in promoting cell growth, we examined whether Pten-NOLC1 regulates gene transcription by exploring the DNA elements that Pten-NOLC1 may interact. We performed a series of chromatin immunoprecipitations (ChIPs) on Pten-NOLC1 knockout cells and their wild-type counterparts with antibodies specific for NOLC1, Pten, and the FLAG tag. DNA fragments in the immunocomplex were extracted and sequenced on an Illumina HiSeq system (ChIP-seq). As shown in figure 5A and supplemental figure 15, 6179 DNA fragment peak events were detected in DU145 cells using an antibody specific for NOLC1, and 2868 peak events were detected in the two *Pten-NOLC1* knockout clones. Similar results were obtained in MCF7 cells: 4347 total peaks in MCF7 cells and 1196 peaks in MKO1 and MKO2 cells. The presence of Pten-NOLC1 is responsible for 2.2- to 3.6-fold increase of DNA targets, obtained through subtraction analysis. To verify whether these DNA binding events are the direct result of *Pten-NOLC1* fusion, we forced Pten-NOLC1 expression in PC3 and RWPE1 cells and found a large number of DNA peaks in the ChIP-seq analysis of these cells reacted with an anti-FLAG antibody. Many peaks overlapped with those found in DU145 and MCF7 cells. The TaqMan qPCR results validated the alignment of the DNA elements (figure 5B) with the gene promoter/enhancer regions of *MET, EGFR*, *RAF1*, *AXL*, *GAB1*, and *VEGFA*

(Supplemental figures 16 and 17). Pathway analysis of these *Pten-NOLC1*-associated DNA fragments suggested that these gene products are among the most enriched molecules in the 'HGF signaling' and 'mechanism of cancer' pathways (Supplemental Tables 10–12).

To determine whether the loss of Pten-NOLC1 alters the expression of these genes, we performed Affymetrix gene expression microarray assays on DU145, DKO1, and DKO2 cells. We found that more than 500 gene transcripts were downregulated in both DKO1 and DKO2 clones compared with their expression levels in the parental DU145 cells. Among these genes, *MET* was downregulated by 2.8-6.0-fold, *EGFR* by 1.4-1.41-fold, *GAB1* by 1.8-1.9-fold, *AXL* by 1.8-2.3-fold, and *VEGFA* by 1.5-1.6-fold (figure 5C). The TaqMan RT-PCR assays validated the down-regulation of these genes. Compared with wild-type MCF7 cells, MCF7 cells with *Pten-NOLC1* knockout exhibited similar downregulation of these genes. Western blot analysis revealed a significant reduction of MET, EGFR, RAF1, and GAB1 expression and very low levels of EGFR, MET, RAF1, and STAT3 phosphorylation in DKO1, and MKO1 cells (figure 5D and supplemental table 13). Interestingly, Pten-NOLC1 knockout also significantly reduced the expression of MDM2, a transcription target of wild type NOLC1, suggesting that Pten-NOLC1 fusion protein may retain significant transcription activity of NOLC1. The re-introduction of *Pten-NOLC1-FLAG* into DKO1 cells led to the reappearance of MET, EGFR, and MDM2 in these cells (figure 5E and supplemental table 13). Taken together, the findings from the ChIP-Seq/microarray and immunoblot analyses suggest that the expression of these ECM, MET, and EGFR signaling molecules involved in cell growth, proliferation, and motility are mainly dependent on the presence of Pten-NOLC1 (figure 5F). Disruption of *Pten-NOLC1* expression in 9 different cancer cell lines, including the DU145, HUH7, HEP3B, MCF7, MB231, and H1299 cell lines, resulted in substantial cell death (Supplemental figure 18 and table 1) but did not impact the *Pten-NOLC1*-negative NIH3T3 cells. Loss of Pten-NOLC1 also showed decreased sensitivity of DU145 cells to the inhibition of a specific EGFR inhibitor (see supplemental results for detail). These results suggest that many cancer cells may addict to *Pten-NOLC1* for survival.

Pten-NOLC1 fusion induces hepatocellular carcinoma in mice

Chromosomal recombination between *Pten* and *NOLC1* results in the concomitant loss of the tumor suppressor gene *Pten* and the generation of *Pten-NOLC1* fusion gene. Some cancers that are positive for Pten-NOLC1 have complete loss of Pten (figure 1B and supplemental table 14). To determine whether this single genetic event is sufficient to generate cancer in mammals, we somatically knocked out *Pten* in the liver of $C57Bl^{loxp\text{-}Pten\text{-}loxp}$ mice via intraperitoneal injection of AAV8-cre followed by hydrodynamic tail vein injection of pT3-*Pten-NOLC1-mCherry* and pSB (figure 6A). Within 18 weeks, six of the seven mice developed hepatocellular carcinoma (Supplemental table 15), showing distinctive tumor nodules in the liver (figure 6B–C). One mouse developed cancer metastasis in the peritoneal cavity. Three animals exhibited the accumulation of ascites. However, none of the control mice with somatic *Pten* knockout and pT3/pSB injection developed tumors during the same period. The tumor cells had large nucleoli and contained significant fat accumulation in the cytoplasm. Besides, the tumor cells displayed a high frequency of Ki-67 staining, an increase of 4.6-fold relative to that in noncancerous

cells (figure 6D). Immunoblot analyses showed that the Pten-NOLC1-mCherry protein was expressed in all cancer samples but was very weak in the liver tissues of mice treated with pT3/pSB and AAV8-cre (figure 6E and supplemental figure 19). All tumor tissues, including the metastatic cancer sample, exhibited upregulation of MET and GAB1. Overall, the results indicate that a single *Pten-NOLC1* fusion event may transform the hepatocytes to the development of spontaneous liver cancer.

Discussion:

Pten deletion and mutation are common drivers in human cancers. Here, we report a *Pten*-derived fusion molecule that functionally promotes cancer cell proliferation and transformation.

Pten-NOLC1-mediated cancer transformation may directly result from the DNA binding and transcriptional activities of the fusion molecule. Our analyses showed that Pten-NOLC1 protein enhanced the expression of several pro-growth signalings, including MET, EGFR, STAT3, GAB1, and RAF1. We found no impacts of Pten-NOLC1 on AKT expression/activation, but *Pten-NOLC1* expression is crucial for cell survival (details in supplemental results and discussion, supplemental figures 20–21, supplemental table 16). As *Pten-NOLC1* knockout cancer cells with MET downregulation exhibit low viability and are not resistant to UV- irradiation-induced cell death. Upregulation of the *MET* pathway by Pten-NOLC1 in the cancer cell line may contribute to the cell resistance to the death signals since the MET-FAS interaction on the membrane that suppresses FAS cell death signaling[29]. The cancer genomes often have a hemizygous *Pten* deletion along with *Pten-NOLC1* genome rearrangement (Supplemental results/discussion, supplemental figure 22 and supplemental table 17), resulting in the cancer cells devoid of Pten activity to deactivate $PI(3,4,5)P_3$ in PI3K/Akt signaling. As a result, the cancers are devoid of functional Pten protein, since Pten-NOLC1 is negative for phospholipid phosphatase activity and translocated to the nucleus. These cancers may have over-activated PI3K/Akt signaling due to the lack of deactivation of $PIP_3(3,4,5)$. To our knowledge, this report is the first to identify a Pten-derived fusion and to characterize Pten-NOLC1 fusion in human cancers. The strategies of random priming in library preparation and the extra-depth coverage (2000x) may be advantageous in detection of 5’ end fusion such as Pten-NOLC1 (see details in supplemental discussion, supplemental figure 23).

The activations of multiple pro-growth signalings, including EGFR by Pten-NOLC1, may contribute to the increased growth rate, resistance to cell death, and transformation of cancer cells. It is still unclear how much each pathway contributes to the cancer phenotype. It appears that each of these pathways may have overlapped and unique roles in generating the cancer cell transformation. The redundancy of the multiple pro-growth signalings promoted by Pten-NOLC1 fusion may reflect a complex signaling mechanism to sustain the cancer phenotype.

The discovery of *Pten-NOLC1* fusion in human cancers has significant clinical implications. Pten-NOLC1 transcriptionally activates MET, EGFR, and other pro-growth signaling molecules. Targeting *Pten-NOLC1* fusion could be an effective cancer treatment. We

recently developed a genome therapy strategy specifically targeting the chromosomal breakpoint of fusion via the CRISPR/*Cas9* system[30]. Indeed, this treatment achieved partial remission of fusion-positive xenograft tumors in animals. The mechanism of chromosome rearrangement that leads to *Pten-NOLC1* fusion is still unclear. The breakpoint of *Pten-NOLC1* in primary cancer samples or cancer cell lines of different organ origins appears identical. The identical genome breakpoint of *Pten-NOLC1* will give significant ease for genome targeting. *Pten-NOLC1* fusion gene may provide an important target for cancer treatment.

Methods:

Tissues and cell lines:

Human samples were obtained in accordance with the guidelines approved by the institutional review boards of the respective institutes. For more information, please see Methods online.

RNA extraction, cDNA synthesis, and TaqMan RT-PCR.

The procedures were previously described[31–36] and were detailed in Methods online.

Detection of the genomic breakpoint of the *Pten-NOLC1* genomic rearrangeme.

Please see Methods online and supplemental table 18 for detail.

Disruption of Pten-NOLC1 via CRISPR/Cas9 genome editing.

The procedure was described in Methods online.

Northern blotting.

The procedure was described in Methods online.

Vectors.

Vectors constructions of pPten-NOLC1-FLAG, pT3-EF1α-Pten-NOLC1, and pGST-Pten-NOLC1 were described in Methods online.

Colony formation and BrdU cell cycle assays.

DU145, MCF7, and H1299 cells or their *Pten-NOLC1* knockout counterparts were analyzed as described in Methods online.

MTT cell proliferation assay.

DU145, MCF7, and their Pten-NOLC1 knockout and rescued counterparts were used with EGFR and MET inhibitors as described in Methods online.

UV-induced cell death FACS assay.

Du145, dKO1, dKO2, MCF7 or mKO1 cells were irradiated with UV and quantified as described in Methods online.

Cell death FACS assay of *Pten-NOLC1* knockout cells.

The procedure was described in Methods online.

Wound-healing and matrigel traverse assays.

The procedures were described in Methods online.

Animal cancer models:

The procedure was described in Methods online.

ChIP-sequencing analysis.

ChIP-sequencing analyses of DU145, MCF7 and their corresponding Pten-NOLC1 knockout counterparts were described in Methods online and supplemental table 19.

Transcriptome sequencing.

Transcriptome sequencing process of PCa, benign prostate tissue adjacent-to-cancer, and prostate organ donor samples were described in Methods online.

Bioinformatic analyses

Fusion transcript detection and TCGA SNP 6.0 data analyses were described in Methods online.

FISH.

The procedures[37–40] were described Methods online.

PI(3,4,5)P_3 phosphatase activity.

The procedures of Pten-NOLC1 and Pten phosphatase assay were described in Methods online.

Nuclear and Nucleolar fractionation.

The procedures of subcellular fractionation were described in Methods online.

Immunoblotting, Immunostaining, immunofluorescence staining and immunoprecipitation.

The antibodies and procedures were described in Methods online.

Supplementary Material

Refer to Web version on PubMed Central for supplementary material.

References:

1. Hanahan D, Weinberg RA. Hallmarks of cancer: the next generation. Cell 2011; 144: 646–674. [PubMed: 21376230]
2. Hanahan D, Weinberg RA. The hallmarks of cancer. Cell 2000; 100: 57–70. [PubMed: 10647931]

3. Luo JH, Liu S, Zuo ZH, Chen R, Tseng GC, Yu YP. Discovery and Classification of Fusion Transcripts in Prostate Cancer and Normal Prostate Tissue. The American journal of pathology 2015.
4. Benson ES. Leukemia and the Philadelphia chromosome. Postgrad Med 1961; 30: A22–A28. [PubMed: 13867350]
5. Tomlins SA, Rhodes DR, Perner S, Dhanasekaran SM, Mehra R, Sun XW et al. Recurrent fusion of TMPRSS2 and ETS transcription factor genes in prostate cancer. Science (New York, NY 2005; 310: 644–648.
6. Kroll TG, Sarraf P, Pecciarini L, Chen CJ, Mueller E, Spiegelman BM et al. PAX8-PPARgamma1 fusion oncogene in human thyroid carcinoma [corrected]. Science (New York, NY 2000; 289: 1357–1360.
7. Chen ZH, Yu YP, Tao J, Liu S, Tseng G, Nalesnik M et al. MAN2A1-FER Fusion Gene Is Expressed by Human Liver and Other Tumor Types and Has Oncogenic Activity in Mice. Gastroenterology 2017; 153: 1120–1132. [PubMed: 28245430]
8. Li J, Yen C, Liaw D, Podsypanina K, Bose S, Wang SI et al. PTEN, a putative protein tyrosine phosphatase gene mutated in human brain, breast, and prostate cancer. Science (New York, NY 1997; 275: 1943–1947.
9. Steck PA, Pershouse MA, Jasser SA, Yung WK, Lin H, Ligon AH et al. Identification of a candidate tumour suppressor gene, MMAC1, at chromosome 10q23.3 that is mutated in multiple advanced cancers. Nature genetics 1997; 15: 356–362. [PubMed: 9090379]
10. Myers MP, Pass I, Batty IH, Van der Kaay J, Stolarov JP, Hemmings BA et al. The lipid phosphatase activity of PTEN is critical for its tumor supressor function. Proceedings of the National Academy of Sciences of the United States of America 1998; 95: 13513–13518. [PubMed: 9811831]
11. Maehama T, Dixon JE. The tumor suppressor, PTEN/MMAC1, dephosphorylates the lipid second messenger, phosphatidylinositol 3,4,5-trisphosphate. The Journal of biological chemistry 1998; 273: 13375–13378. [PubMed: 9593664]
12. Sansal I, Sellers WR. The biology and clinical relevance of the PTEN tumor suppressor pathway. J Clin Oncol 2004; 22: 2954–2963. [PubMed: 15254063]
13. McCubrey JA, Steelman LS, Abrams SL, Lee JT, Chang F, Bertrand FE et al. Roles of the RAF/MEK/ERK and PI3K/PTEN/AKT pathways in malignant transformation and drug resistance. Adv Enzyme Regul 2006; 46: 249–279. [PubMed: 16854453]
14. Baker SJ. PTEN enters the nuclear age. Cell 2007; 128: 25–28. [PubMed: 17218252]
15. Trotman LC, Wang X, Alimonti A, Chen Z, Teruya-Feldstein J, Yang H et al. Ubiquitination regulates PTEN nuclear import and tumor suppression. Cell 2007; 128: 141–156. [PubMed: 17218261]
16. Yin Y, Shen WH. PTEN: a new guardian of the genome. Oncogene 2008; 27: 5443–5453. [PubMed: 18794879]
17. Chen HK, Pai CY, Huang JY, Yeh NH. Human Nopp140, which interacts with RNA polymerase I: implications for rRNA gene transcription and nucleolar structural organization. Molecular and cellular biology 1999; 19: 8536–8546. [PubMed: 10567578]
18. Tsai YT, Lin CI, Chen HK, Lee KM, Hsu CY, Yang SJ et al. Chromatin tethering effects of hNopp140 are involved in the spatial organization of nucleolus and the rRNA gene transcription. Journal of biomedical science 2008; 15: 471–486. [PubMed: 18253863]
19. Renvoise B, Colasse S, Burlet P, Viollet L, Meier UT, Lefebvre S. The loss of the snoRNP chaperone Nopp140 from Cajal bodies of patient fibroblasts correlates with the severity of spinal muscular atrophy. Human molecular genetics 2009; 18: 1181–1189. [PubMed: 19129172]
20. Hwang YC, Lu TY, Huang DY, Kuo YS, Kao CF, Yeh NH et al. NOLC1, an enhancer of nasopharyngeal carcinoma progression, is essential for TP53 to regulate MDM2 expression. The American journal of pathology 2009; 175: 342–354. [PubMed: 19541936]
21. Litovchick L, Sadasivam S, Florens L, Zhu X, Swanson SK, Velmurugan S et al. Evolutionarily conserved multisubunit RBL2/p130 and E2F4 protein complex represses human cell cycle-dependent genes in quiescence. Molecular cell 2007; 26: 539–551. [PubMed: 17531812]

22. Gao X, Wang Q, Li W, Yang B, Song H, Ju W et al. Identification of nucleolar and coiled-body phosphoprotein 1 (NOLC1) minimal promoter regulated by NF-kappaB and CREB. BMB Rep 2011; 44: 70–75. [PubMed: 21266110]
23. Isaac C, Yang Y, Meier UT. Nopp140 functions as a molecular link between the nucleolus and the coiled bodies. The Journal of cell biology 1998; 142: 319–329. [PubMed: 9679133]
24. Pai CY, Chen HK, Sheu HL, Yeh NH. Cell-cycle-dependent alterations of a highly phosphorylated nucleolar protein p130 are associated with nucleologenesis. Journal of cell science 1995; 108 (Pt 5): 1911–1920. [PubMed: 7657714]
25. Li AG, Piluso LG, Cai X, Wei G, Sellers WR, Liu X. Mechanistic insights into maintenance of high p53 acetylation by PTEN. Molecular cell 2006; 23: 575–587. [PubMed: 16916644]
26. Ran FA, Hsu PD, Lin CY, Gootenberg JS, Konermann S, Trevino AE et al. Double nicking by RNA-guided CRISPR Cas9 for enhanced genome editing specificity. Cell 2013; 154: 1380–1389. [PubMed: 23992846]
27. Jinek M, Chylinski K, Fonfara I, Hauer M, Doudna JA, Charpentier E. A programmable dual-RNA-guided DNA endonuclease in adaptive bacterial immunity. Science (New York, NY 2012; 337: 816–821.
28. Lee YM, Miau LH, Chang CJ, Lee SC. Transcriptional induction of the alpha-1 acid glycoprotein (AGP) gene by synergistic interaction of two alternative activator forms of AGP/enhancer-binding protein (C/EBP beta) and NF-kappaB or Nopp140. Molecular and cellular biology 1996; 16: 4257–4263. [PubMed: 8754826]
29. Wang X, DeFrances MC, Dai Y, Pediaditakis P, Johnson C, Bell A et al. A mechanism of cell survival: sequestration of Fas by the HGF receptor Met. Mol Cell 2002; 9: 411–421. [PubMed: 11864613]
30. Chen ZH, Yu YP, Zuo ZH, Nelson JB, Michalopoulos GK, Monga S et al. Targeting genomic rearrangements in tumor cells through Cas9-mediated insertion of a suicide gene. Nature biotechnology 2017; 35: 543–550.
31. Yu YP, Liu P, Nelson J, Hamilton RL, Bhargava R, Michalopoulos G et al. Identification of recurrent fusion genes across multiple cancer types. Sci Rep 2019; 9: 1074. [PubMed: 30705370]
32. Yu Yan-Ping, Tsung Allan, Liu Silvia, Nalesnick Michael, Geller David, Michalopoulos George et al. Detection of fusion transcripts in the serum samples of patients with hepatocellular carcinoma. Oncotarget 2019; In press.
33. Zuo ZH, Yu YP, Martin A, Luo JH. Cellular stress response 1 down-regulates the expression of epidermal growth factor receptor and platelet-derived growth factor receptor through inactivation of splicing factor 3A3. Molecular carcinogenesis 2017; 56: 315–324. [PubMed: 27148859]
34. Chen ZH, Yu YP, Michalopoulos G, Nelson J, Luo JH. The DNA replication licensing factor miniature chromosome maintenance 7 is essential for RNA splicing of epidermal growth factor receptor, c-Met, and platelet-derived growth factor receptor. The Journal of biological chemistry 2015; 290: 1404–1411. [PubMed: 25425645]
35. Yu YP, Michalopoulos A, Ding Y, Tseng G, Luo JH. High fidelity copy number analysis of formalin-fixed and paraffin-embedded tissues using Affymetrix Cytoscan HD chip. PloS one 2014; 9: e92820. [PubMed: 24699316]
36. Yu YP, Tsung A, Liu S, Nalesnick M, Geller D, Michalopoulos G et al. Detection of fusion transcripts in the serum samples of patients with hepatocellular carcinoma. Oncotarget 2019; 10: 3352–3360. [PubMed: 31164957]
37. He DM, Ren BG, Liu S, Tan LZ, Cieply K, Tseng G et al. Oncogenic activity of amplified miniature chromosome maintenance 8 in human malignancies. Oncogene 2017; 36: 3629–3639. [PubMed: 28481876]
38. Yu YP, Ding Y, Chen Z, Liu S, Michalopoulos A, Chen R et al. Novel fusion transcripts associate with progressive prostate cancer. The American journal of pathology 2014; 184: 2840–2849. [PubMed: 25238935]
39. Han YC, Zheng ZL, Zuo ZH, Yu YP, Chen R, Tseng GC et al. Metallothionein 1 h tumour suppressor activity in prostate cancer is mediated by euchromatin methyltransferase 1. The Journal of pathology 2013; 230: 184–193. [PubMed: 23355073]

40. Yu G, Tseng GC, Yu YP, Gavel T, Nelson J, Wells A et al. CSR1 suppresses tumor growth and metastasis of prostate cancer. American Journal of Pathology 2006; 168: 597–607.

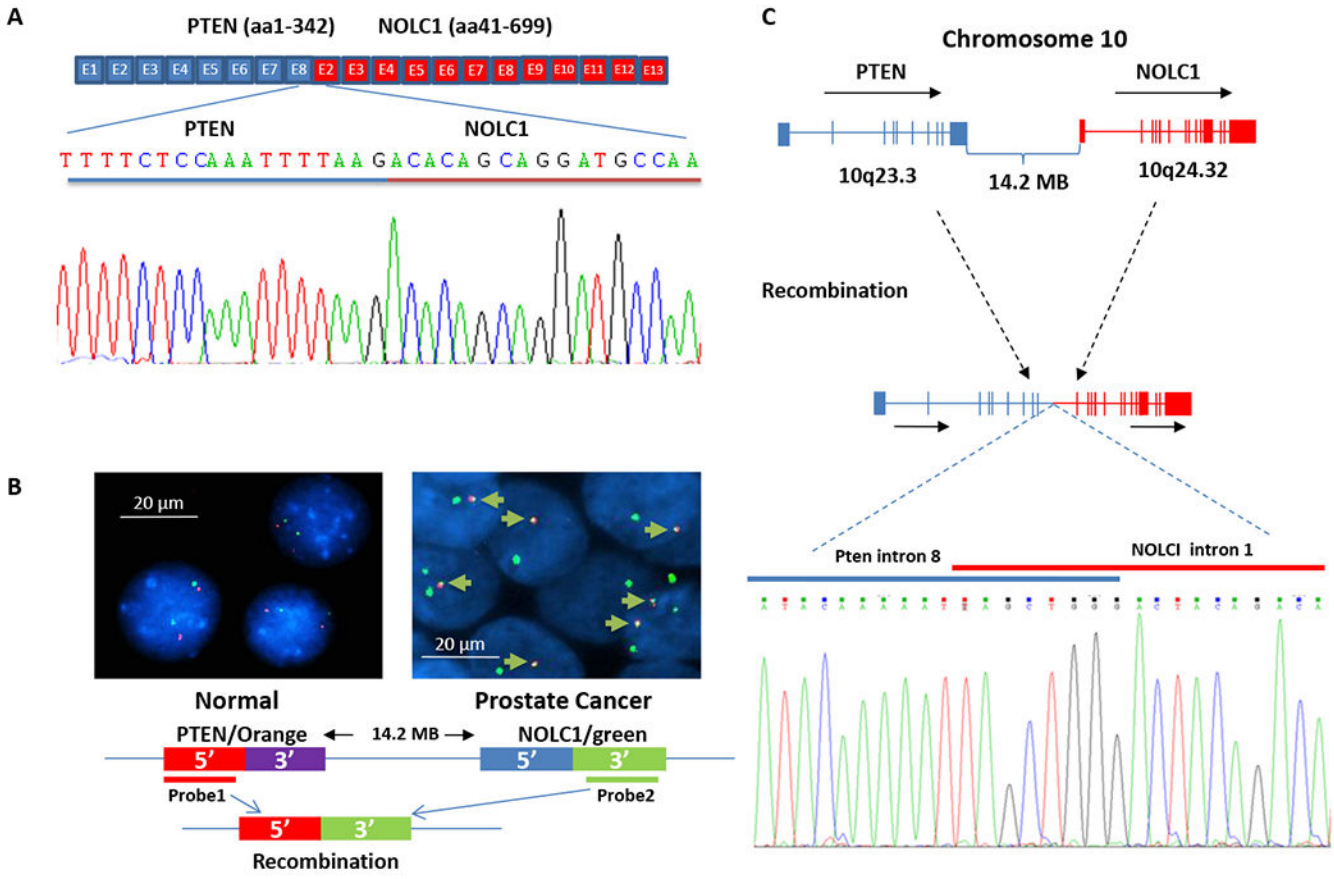

Figure 1. *Pten-NOLC1* fusion.

(A) Schema of *Pten-NOLC1* fusion. Top: Simplified diagrams of the *Pten* and *NOLC1* genomes. The transcription direction, the distance between the fused genes and the fusion direction are indicated. Middle: Representative sequence chromatogram of the fusion transcript with the fusion sequences indicated. Bottom: Diagram of the predicted translation product of the *Pten-NOLC1* fusion transcript. Blue-head gene domain; Red-tail gene domain. (B) Fluorescence *in situ* hybridization (FISH) indicates genomic recombination in PCa cells. Top: Schema of *Pten* and *NOLC1* genomic recombination and the positions of the FISH probe. Bottom: Representative FISH images for normal prostate epithelial cells (DO12) and cancer cells positive for the *Pten-NOLC1* fusion gene: orange-probe 1; Green-probe 2; Green arrows-fusion signals. (C) Genomic breakpoint analysis of *Pten-NOLC1* fusion. Schema of Pten and NOLC1 genome joining and representative sequence chromatogram is shown.

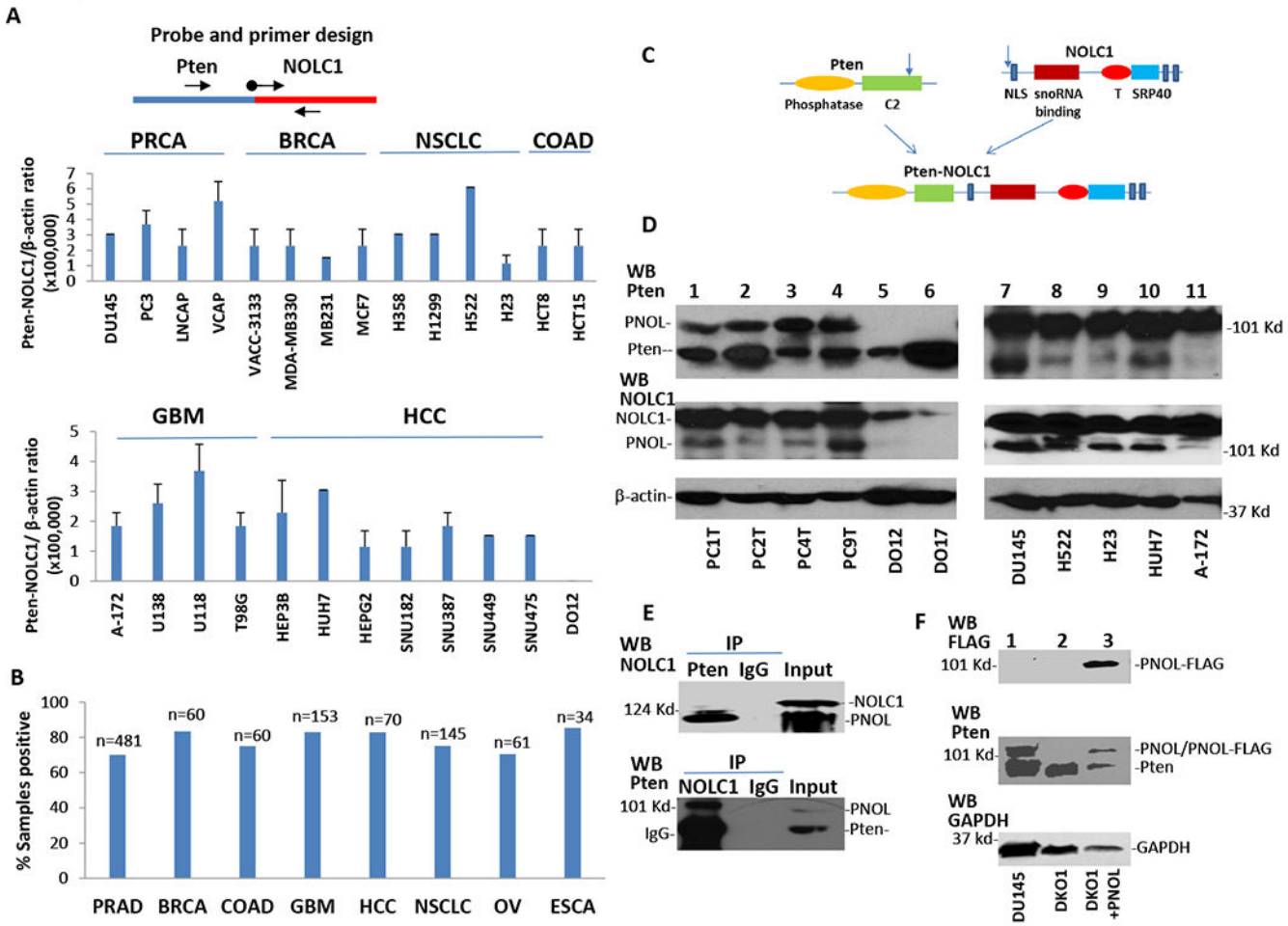

Figure 2. *Pten-NOLC1* fusion in human cancers.

(A) *Pten-NOLC1* was found in 26 human cancer cell lines but not in healthy prostate donor samples by TaqMan qRT-PCR. All positive samples were confirmed by Sanger sequencing. (B) Detection frequency of *Pten-NOLC1* in primary human tumor samples. The numbers of samples are indicated. Twenty-five percent positive samples were confirmed by Sanger's sequencing. (C) Diagram of the functional domains of the Pten and NOLC1 proteins as well as the Pten-NOLC1 fusion protein. The arrows indicate the truncation sites. NLS - nuclear signal sequences; SRP40 - domain homologous to the C-terminus of the *S. cerevisiae* SRP40 protein; snoRNA binding - binding site for small nucleolar RNA; T - serine-rich sequence homologous to the HSV1 transcription factor ICP4. (D) Detection of Pten-NOLC1 by immunoblotting with antibodies specific for Pten (upper panel), NOLC1 (middle panel) and β-actin in prostate cancers (PC1T, PC2T, PC4T, and PC9T), prostate organ donors (DO12 and DO17) and human cancer cell lines (lanes 7-11). PNOL denotes Pten-NOLC1. (E) Immunoprecipitation and immunoblotting to identify the Pten-NOLC1 protein in DU145 cells. Top: Protein lysates from DU145 cells were immunoprecipitated with Pten antibody and immunoblotted with NOLC1 antibody. Immunoprecipitation with nonspecific IgG was used as the negative control. Bottom: Protein lysates from DU145 cells were immunoprecipitated with NOLC1 antibody and immunoblotted with Pten antibody.

Nonspecific IgG immunoprecipitation is the negative control. (F) Identification of Pten-NOLC1 in DU145 cells and derivative cell lines. Protein lysates from DU145 cells (lane 1), DU145 with Pten-NOLC1 disruption (DKO1, lane 2), and Pten-NOLC-FLAG-rescued KO1 cells (lane 3; DKO1+PNOL) were immunoblotted with FLAG (top) or Pten (middle) antibody. Lysate immunoblotted with GAPDH antibody was used as the normalization control (bottom). PNOL denotes the Pten-NOLC1 protein.

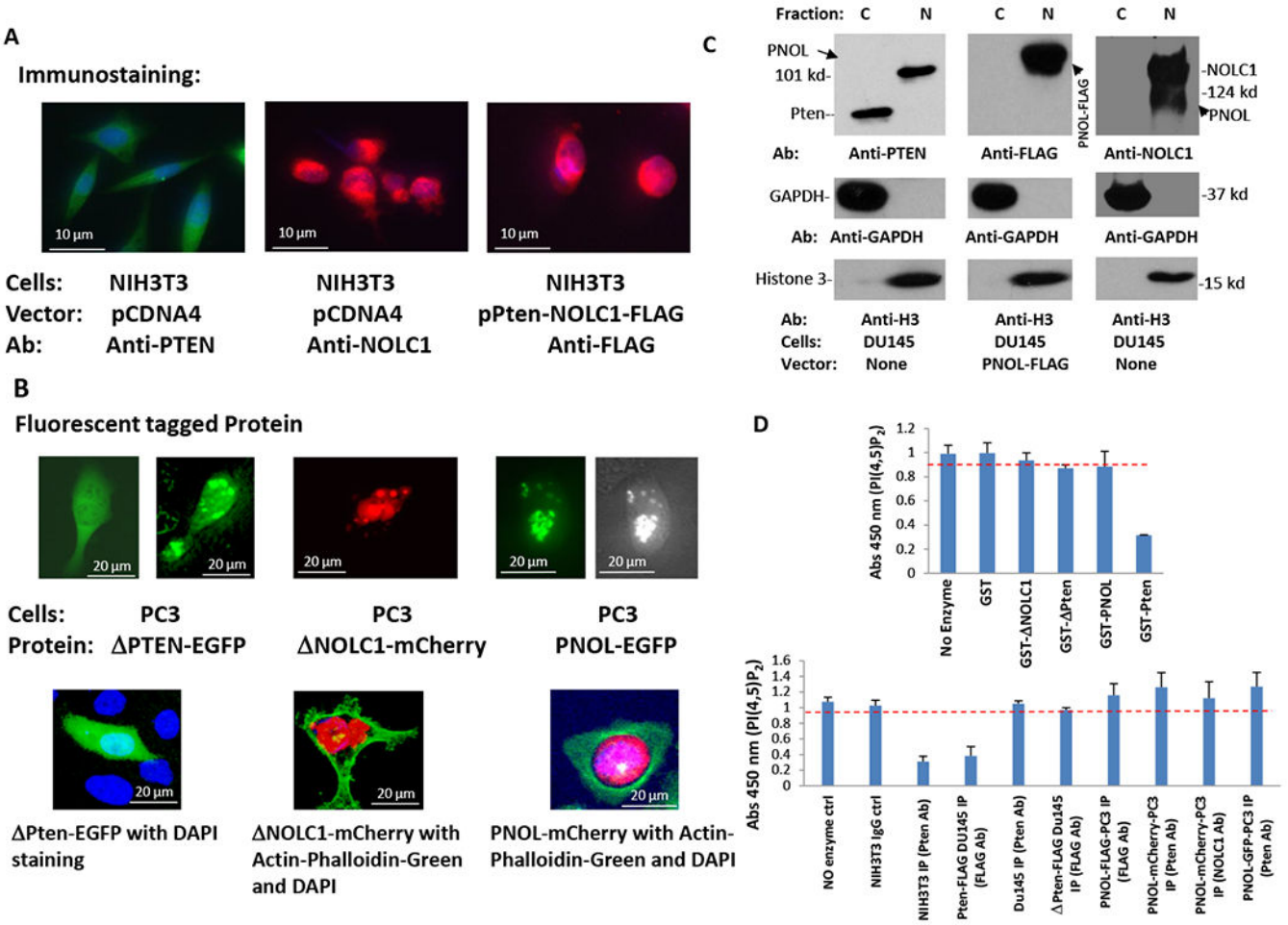

Figure 3. Pten-NOLC1 is localized in the nucleus and lacks PIP_3 phosphatase activity.

(A) Immunostaining of NIH3T3 cells with antibodies specific for Pten (left, FITC), NOLC1 (middle, Cy5) or FLAG (Pten-NOLC1-FLAG) (right, Cy5). (B) Fluorescent chimera proteins of ΔPten$^{aa1\text{-}342}$, Pten-NOLC1 and ΔNOLC1$^{aa41\text{-}699}$. Upper panel: Live cell imaging of PC3 cells transfected with p*ΔPten$^{aa1\text{-}342}$-EGFP* (left), p*ΔNOLC1C$^{aa41\text{-}699}$-mCherry* (middle) and p*Pten-NOLC1-EGFP* (right). Lower panel: Confocal images of PC3 cells transfected with p*ΔPten$^{aa1\text{-}342}$-EGFP* and co-stained with DAPI to identify nuclei (left), or with p*ΔNOLC1C$^{aa41\text{-}699}$-mCherry* and co-stained with DAPI and actin-phalloidin green (APG, middle), or with p*Pten-NOLC1- mCherry* and co-stained with DAPI and APG (right). (C) Immunoblotting of Du145 cellular fractions. Antibodies specific for Pten, NOLC1, and FLAG detected Pten-NOLC1 (110 kd) in the nuclear (25% of total nuclear fraction loaded) or cytoplasmic fraction (10% of total cytosolic fraction from 5x10^6 cells loaded). GAPDH and Histone 3 antibodies were used to assess the purity of the fractions. (D) Pten-NOLC1 lacks Pten phosphatase activity *in vitro*. Upper: The PIP_3 phosphatase activity of purified GST, GST-Pten-NOLC1 (GST-PNOL), GST-Pten, GST-ΔPten$^{aa1\text{-}342}$ (GST-ΔPten), and GST-ΔNOLC1$^{aa41\text{-}699}$ (GST-ΔNOLC1) proteins. Lower: immunopurified Pten from NIH3T3 (NIH3T3 IP) or IgG control, immunopurified Pten-FLAG from Pten-FLAG transformed DU145 (Pten-FLAG DU145 IP) using FLAG antibody, immunoprecipitates from DU145

(DU145 IP) using Pten Ab, immunopurified ΔPten-FLAG from $\Delta Pten^{aa1\text{-}342}$-FLAG transformed DU145 cells (ΔPten-FLAG Du145 IP) using FLAG antibody, immunopurified Pten-NOLC1-FLAG from Pten-NOLC1-FLAG transformed PC3 cells (PNOL-FLAG-PC3 IP) using FLAG antibody, immunopurified Pten-NOLC1-mCherry from Pten-NOLC1-mCherry transformed PC3 cells (PNOL-mCherry-PC3 IP) using Pten antibody, immunopurified Pten-NOLC1-mCherry from Pten-NOLC1-mCherry transformed PC3 cells (PNOL-mCherry-PC3 IP) using NOLC1 antibody, and immunopurified Pten-NOLC1-GFP from Pten-NOLC1-GFP transformed PC3 cells (PNOL-GFP-PC3 IP) using Pten antibody. These immunoprecipitates were analyzed via ELISA. The resulting Pten activity was inversely proportional to the absorbance of 450 nm for $PI(4,5)P_2$ in the competitive binding experiment. Each data point is the average of three independent experiments with triplicate samples. A measurement value below the threshold (red dotted line) indicates positive PIP3 phosphatase activity, while a value at or above the threshold indicates negative activity.

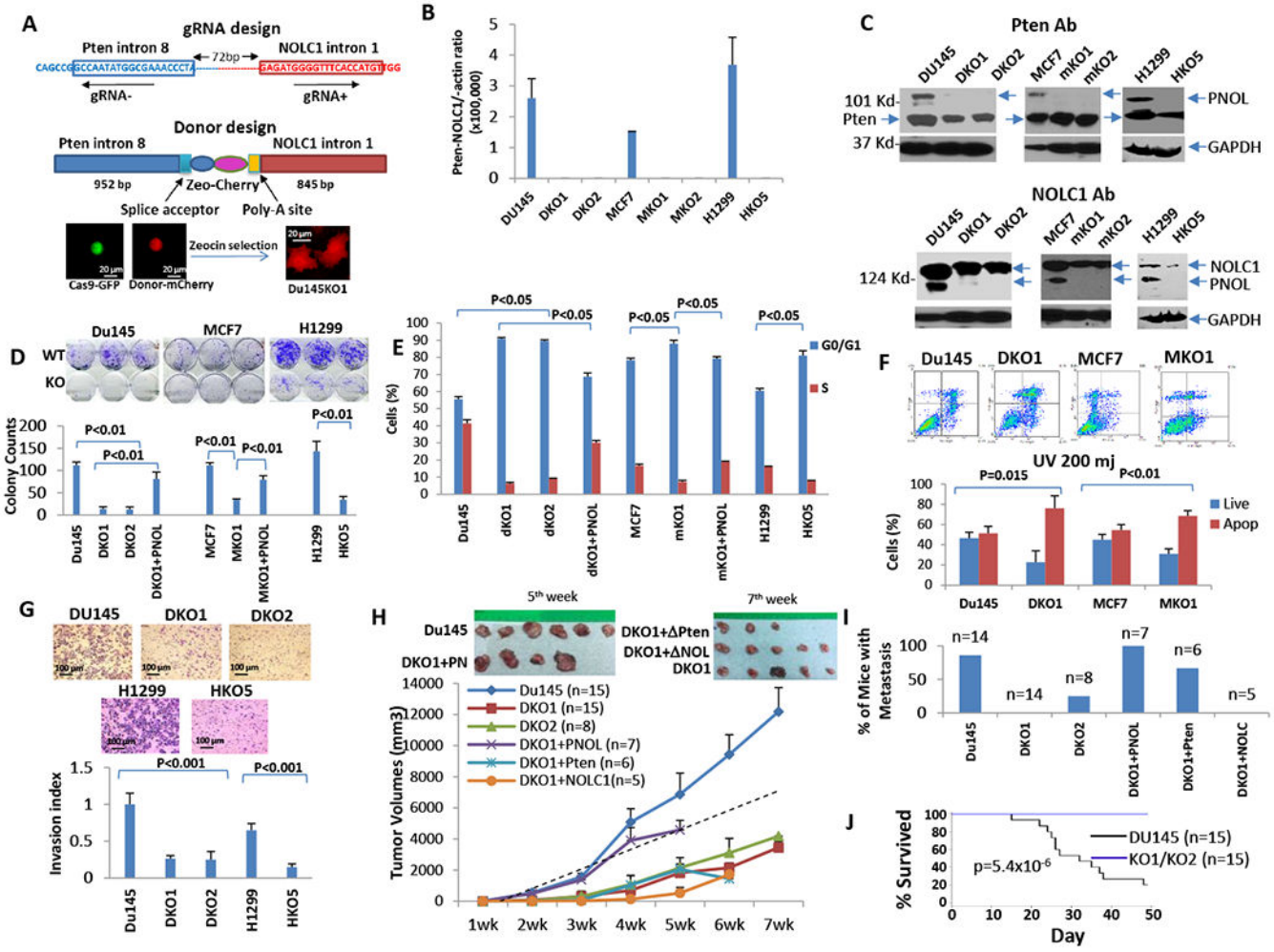

Figure 4. Pten-NOLC1 promotes cancer cell growth and invasion *in vitro* and *in vivo*.

(A) Schema of the *Pten-NOLC1* knockout strategy. Top: sgRNA design. Middle: Donor vector design. Bottom: Images of Cas9^{D10A}-EGFP and Zeocin-mCherry coexpression in DU145 cells after cotransfection of the pCas9^{D10A}-EGFP-gRNA and pPten^{intron8}-Zeocin-mCherry-NOLC1^{intron1} vectors. (B) Detection of *Pten-NOLC1* RNA in *Pten-NOLC1* knockout clones via TaqMan RT-PCR. TaqMan qRT-PCR was performed on RNA extracts from DKO1/ DKO2 cells (DU145 cells with *Pten-NOLC1* knockout), MKO1/MKO1 cells (MCF7 cells with *Pten-NOLC1* knockout), and HKO5 cells (H1299 cells with *Pten-NOLC1* knockout). β-Actin was used as the normalization control. (C) Immunoblotting analyses of Pten-NOLC1 expression in Pten-NOLC1 knockout clones. Protein extracts from DKO1, DKO2, MKO1, MKO1 and HKO5 cells and the corresponding wild-type Du145, MCF7 and H1299 cells were immunoblotted with antibodies specific for Pten (left) or NOLC1 (right). Immunoreactions with GAPDH antibody were used as the normalization control. (D) *Pten-NOLC1* promoted colony formation. The insets: Examples of the colony formation assays: DU145/DKO1, MCF7/MKO1, and H1299/HKO5 cells. Each bar represents the mean of three independent experiments of triplicate samples. The standard deviations and p-values <0.01 are indicated. (E) *Pten-NOLC1* promoted cell entry into S phase. The insets:

Examples of BrdU labeling of 10,000 cells of the indicated cell types. Each bar represents the mean of three independent experiments with triplicate samples. The standard deviations and p-values <0.05 are indicated. (F) Pten-NOLC1 enhanced resistance to UV-induced cell death. The insets: Examples of Annexin V and PI staining of cells after exposure to UV radiation (175 MJ). Each bar represents the mean of three independent experiments with triplicate samples. Standard deviations and p-values are indicated. (G) Knockout of *Pten-NOLC1* reduced cancer cell invasion. The invasion indexes were calculated as the ratio of cells migrated through the membrane/cells migrated through the control insert. Each bar represents the means of three independent experiments with triplicate samples. The standard deviations and p-values <0.001 are indicated. (H) *Pten-NOLC1* increased the volume of xenograft tumors. The volumes of xenograft tumors of the indicated cells are plotted. The number of animals in each group is indicated. The inset on the left shows the tumors generated by DU145 and DKO1+Pten-NOLC1 (PN) cells five weeks after xenograft, and the inset on the right shows the tumors generated by DKO1, DKO1+ΔPten, and DKO1+ΔNOLC1 (ΔNOL) cells seven weeks after xenograft. (I) Expression of *Pten-NOLC1* enhanced metastasis. (J) Disruption of Pten-NOLC1 improved the survival of animals xenografted with DU145 cells.

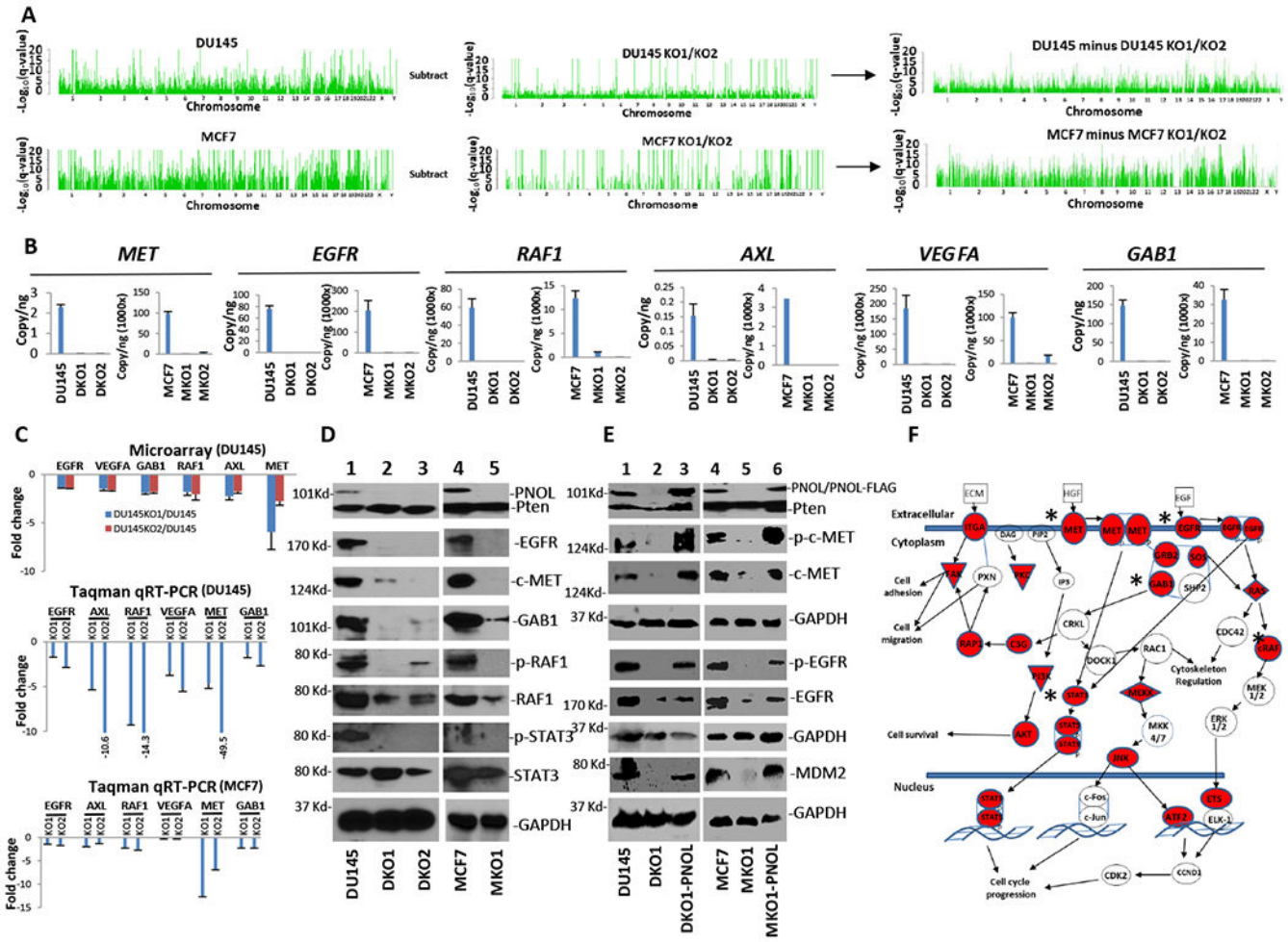

Figure 5. Pten-NOLC1 interacts with genomic DNA and activates the expression of progrowth genes.

(A) Genome distribution of mapped DNA fragments from ChIP-seq of DU145 versus DU145 KO1/KO2 cells (top) and MCF7 versus MCF7 KO1/KO2 cells (bottom) using NOLC1 antibody. The distributions of DNA fragments in DU145 or MCF7 cells after subtraction from the profiles of their knockout counterparts are shown in the right. (B) TaqMan qPCR quantification of Pten-NOLC1 binding to promoter/enhancer regions of *MET*, *EGFR*, *RAF1*, *AXL*, *GAB1*, and *VEGFA*. (C) disruption of *Pten-NOLC1* induced the downregulation of *EGFR*, *VEGFA*, *GAB1*, *EREG*, *AXL*, and *c-MET*. Top: Microarray analysis; Middle: TaqMan qRT-PCR of *EGFR*, *AXL*, *EREG*, *VEGFA*, *c-MET*, and *GAB1* in DU145 cells and their *Pten-NOLC1* knockout counterparts. Expression changes of *Pten-NOLC1* knockout clones relative to DU145 cells are shown. Standard deviations from three independent experiments are indicated. Bottom: TaqMan qRT-PCR of *EGFR*, *AXL*, *EREG*, *VEGFA*, *c-MET*, and *GAB1* in MCF7 cells and their *Pten-NOLC1* knockout counterparts. Fold changes in expression are shown. Standard deviations from three independent experiments are indicated. (D) Deletion of *Pten-NOLC1* in PC3 and MCF7 cells reduced c-MET, EGFR, RAF1, and GAB1 protein expression and STAT3 and RAF1 phosphorylation. (E) Rescue of DKO1 and MO1 cells with Pten-NOLC1 restored the expression of c-MET,

EGFR, and their phosphorylations (pY1234/1235 for c-MET and pY1068 for EGFR) as well as MDM2. (F) The *MET*, *EGF*, and *ECM* signaling pathways were impacted by the presence of *Pten-NOLC1*. The red icons indicate genes interacting with the Pten-NOLC1 proteins but not the NOLC1 protein. *-validated event.

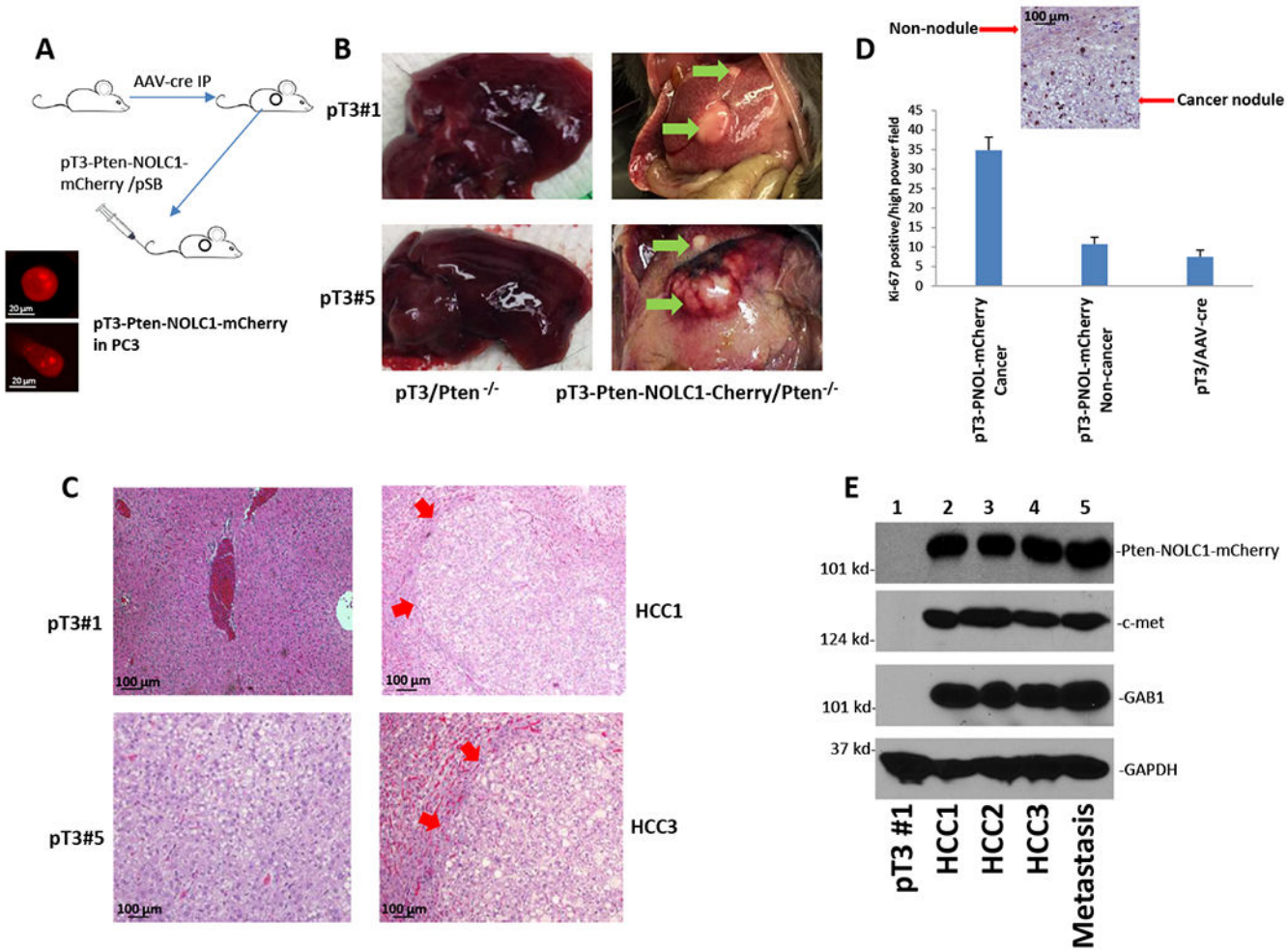

Figure 6. ***Pten-NOLC1*** **fusion generates spontaneous liver cancer.**

(A) *Pten-NOLC1* animal model: Pten was deleted somatically through the treatment of C57Bl$^{loxp\text{-}Pten\text{-}loxp}$ mice with AAV8-cre, followed by hydrodynamic tail vein injection of pT3-Pten-NOLC1-mCherry/pSB. The insets: Examples of PC3 cells transfected with pT3-Pten-NOLC1-mCherry/pSB. (B) Examples of livers from mice treated with AAV8-cre and pT3-Pten-NOLC1-mCherry/pSB (right) or treated with AAV8-cre and pT3/pSB (left). The arrows indicate liver cancer nodules. (C) Hematoxylin and eosin staining of two liver cancer samples (HCC1 and HCC3) from pT3-Pten-NOLC1-mCherry/pSB-treated mice (right) and two control samples (pT3#1 and pT3#5) from pT3/pSB-treated mice (left). The red arrows indicate the tumor nodules. (D) Immunostaining of tumor tissues from pT3-Pten-NOLC1-mCherry/pSB-treated mice with Ki-67 antibody. The bar graphs show the mean numbers of Ki-67-positive tumor cells in 7 high power fields (20x). (E) Increased expression of c-MET and GAB1 in mouse liver cancer samples (HCC1, HCC2, HCC3, and Metastasis) was mediated by *Pten-NOLC1* gene fusion. Liver samples from pT3/pSB (pT3#1)-treated mice were used as the control.

Table 1

Induction of cell death by disruption of Pten-NOLC1

Cell line	$Cas9^{D10A}$ only	$Cas9^{D10A}$ + gRNAs	$Cas9^{D10A}$ + gRNAs + KO cassette
	% cell death	% cell death	% cell death
MDA-MB231	17.6 ± 0.50	20.0 ± 0.73	49.8 ± 0.83
MCF7	44.8 ± 2.41	44.7 ± 1.25	72.7 ± 0.47
PC3	11.2 ± 0.34	40.7 ± 0.94	66.1 ± 0.82
DU145	29.6 ± 1.74	30.0 ± 0.05	57.7 ± 1.25
SNU475	10.4 ± 2.41	29.5 ± 0.75	70.3 ± 0.97
HEP3B	35.7 ± 0.22	42.9 ± 0.25	49.6 ± 0.25
SNU449	11.7 ± 0.45	21.6 ± 0.42	49.5 ± 2.31
H1299	19.3 ± 0.43	58.2 ± 0.97	73.6 ± 8.38
NIH3T3	15.5 ± 0.46	16.0 ± 0.21	18.9 ± 0.34